NREL/SR-520-23543 • UC Category: 1262

Amorphous Silicon Research

Phase III Technical Progress Report
1 August 1996 - 31 July 1997

S. Guha
United Solar Systems Corporation
Troy, Michigan

NREL technical monitor: K. Zweibel

National Renewable Energy Laboratory
1617 Cole Boulevard
Golden, Colorado 80401-3393
A national laboratory of
the U.S. Department of Energy
Managed by Midwest Research Institute
for the U.S. Department of Energy
under Contract No. DE-AC36-83CH10093

Prepared under Subcontract No. ZAN-4-13318-02

November 1997

NOTICE

Available to DOE and DOE contractors from:
Office of Scientific and Technical Information (OSTI)
P.O. Box 62
Oak Ridge, TN 37831
Prices available by calling (423) 576-8401

Available to the public from:
National Technical Information Service (NTIS)
U.S. Department of Commerce
5285 Port Royal Road
Springfield, VA 22161
(703) 487-4650

Preface

This Annual Technical Progress Report covers the work performed by United Solar Systems Corp. for the period 1 August 1996 to 31 July 1997 under DOE/NREL Subcontract No. ZAN-4-13318-02. The following personnel participated in the research program.

A. Banerjee, E. Chen, K. Downs, T. Glatfelter, S. Guha (Principal Investigator), H. Laarman, M. Haag, G. Hammond, M. Hopson, T. Palmer, S. Sugiyama, D. Wolf, J. Yang, and K. Younan.

We would like to thank V. Trudeau for preparation of this report.

Executive Summary

Objectives

The principal objective of this R&D program is to expand, enhance and accelerate knowledge and capabilities for the development of high-performance, two-terminal multijunction hydrogenated amorphous silicon (a-Si) alloy cells and modules. The near-term goal of the program is to achieve 12% stable active-area efficiency using the multijunction approach. The long-term goal is to achieve 15% stable efficiency multijunction modules.

Approach

The major effort of this program is to develop high efficiency component cells and incorporate them in the triple-junction structure to obtain the highest stable efficiency. New and improved deposition regimes were investigated to obtain better cell performance. Fundamental studies to obtain better understanding of material and cell performance were undertaken.

Status/Accomplishments

- We carried out a series of experiments using discharge modulation at various pulsed-plasma intervals in order to study the effect of Si-particle incorporation on solar cell performance. We found no observable difference in cell performance under discharge modulated and standard conditions for deposition regimes investigated.

- We conducted a series of temperature ramping experiments on samples prepared with high and low hydrogen dilutions in order to study the effect of hydrogen effusion on solar cell performance. We found that hydrogen effusion in highly diluted samples resulted in little change in cell efficiency, but caused a reduction in cell performance in low dilution samples.

- We replaced hydrogen with deuterium and found deuterated amorphous silicon alloy solar cells exhibit reduced light-induced degradation. The deuterated alloys have structural similarity with hydrogenated alloys grown with heavy hydrogen dilution. The improved stability is believed to arise from improved microstructures.

- We achieved a world record single-junction a-Si alloy stable cell efficiency of 9.2% with an active-area of 0.25 cm^2 grown with high hydrogen dilution.

- We achieved state-of-the-art top, middle, and bottom component cells with the initial and stable characteristics shown in Table I.

- We achieved a world record triple-junction, stable, active-area cell efficiency of 13.0% with an active area of 0.25 cm^2. The J-V characteristics are shown in Table I. Table I also lists progress made in cell efficiencies since the beginning of the subcontract.

Table I. **Initial and Light-soaked J-V Characteristics of the Component and Triple-junction Cells at United Solar.**

Cell	Status	J_{sc} (mA/cm^2)	V_{oc} (V)	FF	P_{max} (mW/cm^2)
top[d]	initial[a]	8.97	0.980	0.761	6.69
middle[e]	initial[b]	9.30	0.753	0.687	4.81
bottom[f]	initial[c]	12.2	0.631	0.671	5.17
triple[d]	initial[c]	8.57	2.357	0.723	14.6
top[d]	1994 stable[b]	7.3	0.97	0.72	5.1
	1997 stable[a]	8.78	0.953	0.709	5.93
middle[e]	1994 stable[b]	7.6	0.76	0.60	3.5
	1997 stable[b]	8.92	0.717	0.587	3.75
bottom[f]	1994 stable[c]	9.84	0.67	0.55	3.60
	1996 stable[c]	11.4	0.60	0.56	3.80
	1997 stable[c]	11.12	0.609	0.622	4.21
triple[d]	1995 stable[c]	6.87	2.38	0.68	11.1
	1996 stable[c]	7.49	2.283	0.692	11.8
	1997 stable[c]	8.27	2.294	0.684	13.0

a deposited on a bare stainless steel substrate
b deposited on a textured substrate coated with Cr
c deposited on textured Ag/ZnO back reflector
d measured under AM1.5 illumination
e measured under AM1.5 with a λ>530 nm filter
f measured under AM1.5 with a λ>630 nm filter

Table of Contents

List of Figures

List of Tables

Section 1

Introduction

This report describes the research performed during Phase III of a three-phase, three-year program under NREL Subcontract No. ZAN-4-13318-02. The program has now been extended for another seven months, which will constitute Phase IV of the project. The research program is intended to expand, enhance and accelerate knowledge and capabilities for the development of high-performance, two-terminal multijunction amorphous silicon (a-Si) alloy cells and modules.

It is now widely recognized that a multijunction, multibandgap approach has the potential of achieving the highest stable efficiency in a-Si alloy solar cells. In this approach, the bandgap of the materials of the component cell is varied in order to capture a wide spectrum of the solar photons. Significant progress has been made in the development of materials and cell design in the last few years, and a stable module efficiency of 10.2% has been demonstrated over one-square-foot area using a triple-junction approach in which the bottom two component cells use amorphous silicon germanium (a-SiGe) alloy. In order to meet the Department of Energy goal of achievement of 15% stable module efficiency, it is necessary to make further improvements in each of the component cells. This has been the thrust of the current program.

It is well-recognized that plasma chemistry, choice of precursors, growth kinetics, and hydrogen bonding play important roles in determining material properties. In Section 2, we investigate the effect of particulates in the plasma on cell properties. The density of particulates was controlled by modulation of the discharge during deposition. To understand the role of hydrogen bonding on cell properties, we have investigated the effect of hydrogen effusion on cell performance for cells grown with low and high hydrogen dilution. The results, both for initial and light-degraded states, are presented in Section 3. We have also replaced hydrogen with deuterium in the deposition gas mixtures and investigated the effect on cell performance and stability. The results are presented in Section 4 where a possible correlation between stability and microstructure of the material is discussed.

In Section 5, we present the status of the component cell performance; incorporation of these component cells to design a high-efficiency, triple-junction cell is discussed in Section 6. Light-induced degradation studies are presented and the achievement of a new world record of 13% stable active-area cell efficiency is reported. The performance of the triple-junction cells as a function of temperature is also discussed. In Section 7, we comment on the future directions of research.

Section 2

Effect of Discharge Modulation on a-Si Alloy Solar Cells

Gallagher et al. proposed (Gallagher et al. 1996) that the incorporation of Si particles into a-Si alloy films can affect electrical quality of the films. They also suggest that it is possible to reduce the particles by using discharge modulation during deposition.

In order to investigate the effect of Si-particles' incorporation in a-Si alloy solar cells, we fabricated *p-i-n* a-Si alloy solar cells on stainless steel substrates where intrinsic layers were deposited by using pulsed-rf plasma with period of 1 ms, 10 ms, and 100 ms, and compared the characteristics with those of the reference cells made by continuous rf plasma; the deposition conditions are otherwise the same. The duty cycle of the pulse is fixed at 50% for all experiments.

The initial characteristics of the cells are listed in Table II. The deposition time is adjusted to obtain the same thickness. We could achieve stable plasma for 1 ms and 10 ms pulses. For the 100 ms pulse, the plasma became unstable after ~8 min of deposition. From Table II, the characteristics of the cells using pulsed plasma seem to be similar to that by continuous plasma.

Table II. Cell Characteristics for Different Pulsed Conditions Described in the Text.

Run #	Pulse	i-D time (min)	Thickness (Å)	P_{max} (mW/cm^2)	J_{sc} (Q) (mA/cm^2)	V_{oc} (V)	FF	Blue	Red	Comments
6555	No-)	8.6	2250	7.26	12.21	0.951	0.625	0.754	0.660	
6576	pulse)	8.6	2390	7.28	11.83	0.926	0.665	0.755	0.707	
6567	1 ms)	16	2230	7.06	12.36	0.941	0.607	0.753	0.650	
6592	pulse)	17.5	2200	6.77	12.07	0.920	0.610	0.739	0.639	
6566	10 ms pulse	13	2280	6.89	11.66	0.944	0.626	0.747	0.667	
6553	100 ms pulse	13	2360	7.59	12.22	0.944	0.658	0.764	0.700	plasma unstable

We also adjusted the rf power to obtain the same *i*-layer thickness for no pulse, 1 ms, and 100 ms pulses while keeping the deposition time constant. The initial characteristics are listed in Table III. This result also shows that there is no observable difference between pulsed plasma and continuous plasma.

We are planning to investigate Si-particle incorporation under 1 ms, 10 ms, and 100 ms pulsed conditions using atomic force scanning microscopy and will report our findings in the future.

Table III. Cell Characteristics for Different Pulsed Conditions Described in the Text.

Run #	Pulse	i-D.time (min)	Temp. (°C)	Thickness (Å)	P_{max} (mW/cm²)	J_{sc} (Q) (mA/cm²)	V_{oc} (V)	FF	Blue	Red
6534	No-Pulse	7	300	1530	6.56	9.87	0.959	0.693	0.753	0.713
6538	1 ms Pulse	7	300	1650	6.86	10.19	0.957	0.703	0.762	0.712
6539	100 ms Pulse	7	300	1620	6.38	9.47	0.961	0.701	0.754	0.712

Section 3

Effect of Hydrogen Effusion on a-Si Alloy Solar Cells

Amorphous silicon alloy solar cells prepared with high hydrogen dilution have been found to be more stable than those prepared with low dilution. Films with high dilution also exhibit a sharp peak at low temperature (400 °C) in hydrogen effusion spectra. To study the effect of hydrogen effusion on solar cell performance, we have prepared two sets of a-Si alloy *p i n* solar cells on ss with high and low hydrogen dilutions. In the high dilution case, we prepared one cell with standard procedures and two other cells in which the sample temperature was raised to 400 °C at two different rates after the *i* layer deposition. In the low dilution case, only one effusion sample and one standard sample were prepared. The results are summarized in Table IV.

Table IV. Initial Characteristics of a-Si Alloy *p i n* Solar Cells with and without Hydrogen Effusion Prepared with High and Low Hydrogen Dilution.

Run #	H_2-Effusion after *i* dep.	P_{max} (mW/cm²)	J_{sc} (mA/cm²)	V_{oc} (V)	FF	Thickness (Å)	Notes
6424	No	6.60	8.52	1.014	0.764	1250	*i* dep. temp.: 150°C
6422	H_2-Effusion (1)	6.65	9.09	0.985	0.743	1170	**High H-dilution**
6423	H_2-Effusion (2)	6.56	8.84	0.990	0.750	1230	For all samples
6431	No	5.43	7.38	0.983	0.746	1020	*i* dep. temp.: 200°C
6430	H_2-Effusion (1)	5.03	7.16	0.961	0.731	950	**Low H-dilution** For both samples

Condition of H_2-Effusion after *i*-layer deposition

H_2-Effusion (1): Temperature increased at 10 °C/6 min up to 400 °C (similar to earlier hydrogen effusion experiment).

H_2-Effusion (2): Temperature increased up to 400 °C rapidly, then maintained at 400 °C for 15 min.

It is observed that

1. For the cells with high hydrogen dilution, hydrogen effusion after *i* layer deposition under H_2-Effusion (1) condition gives lower V_{oc} and FF but higher J_{sc}, resulting in similar efficiencies (6422-6424). On the other hand, for cells with low dilution, all characteristics seem to become poorer with hydrogen effusion (compare 6430 to 6431). It is interesting to note that highly diluted cells after hydrogen effusion give rise to higher J_{sc} although the low dilution cell did not show this behavior. It should also be pointed out from our earlier experiments that low hydrogen dilution film did not show sharp H_2 effusion peak at low temperatures.

2. More hydrogen is effused out by using H_2-Effusion (1) than H_2-Effusion (2).

As shown in Table V, light-soaking experiments show that cells with H_2-effusion after *i*-layer deposition have higher degradation than the one without H_2-effusion as reflected in the fill factor. It appears that hydrogen in the film which is effused out at lower temperature (~400 °C) affects cell stability. We do not know if the effused-out hydrogen is bonded or nonbonded. More experiments are certainly needed to understand the effect of hydrogen effusion on cell performance.

Table V. Light Soaking Behavior of Cells with and without Hydrogen Effusion.

Run #	H_2-Effusion after *i* dep.	State	P_{max} (mW/cm^2)	J_{sc} (mA/cm^2)	V_{oc} (V)	FF	Thickness (Å)
6424	No	Initial	6.60	8.52	1.014	0.764	1250
		Stable (1010 hrs)	5.63	8.17	0.977	**0.705**	
		Degradation	15%	4%	4%	8%	
6422	H_2-Effusion (1)	Initial	6.65	9.09	0.985	0.743	1170
		Stable (1010 hrs)	5.45	8.66	0.940	**0.670**	
		Degradation	18%	5%	5%	10%	
6423	H_2-Effusion (2)	Initial	6.56	8.84	0.990	0.750	1230
		Stable (1010 hrs)	5.42	8.50	0.948	**0.673**	
		Degradation	17%	4%	4%	10%	

See Table IV for H_2-Effusion (1) and H_2-Effusion (2) conditions.

Section 4

Stability Study of a-Si:D and a-Si:H *p i n* Alloy Solar Cells

Introduction

Light-induced degradation of hydrogenated amorphous silicon (a-Si:H) alloy materials and devices has been the subject of intensive studies. It is generally agreed that recombination of excess electron-hole pairs generated by illumination creates metastable defects in the bulk of the material (Guha et al. 1983). The defect states reduce the mobility-lifetime of the carriers and causes degradation of solar cell performance. The origin of the metastability is not quite understood, and the list of possible causes includes (Wronski and Maley 1991) hydrogen, impurities such as O, N, and C, microvoids, weak bond, or a combination of these. The possible involvement of hydrogen in the light degradation process has motivated several workers to replace hydrogen with its isotope, deuterium, in the a-Si alloy and to investigate stability issues. Stutzmann et al. (Stutzmann et al. 1986) studied the spin density after light exposure for both deuterated and hydrogenated alloys and came to the conclusion that light-induced degradation in both the materials is similar. In a series of experiments, Ganguly et al. (Ganguly et al. 1990, 1991, 1994) have studied light-induced changes in photoconductivity and defect density in hydrogenated and deuterated alloys deposited by using SiH_4 or SiD_4 gases. They reported that in the degraded state, photoconductivity was higher in the deuterated alloy although the defect density from constant photocurrent method (CPM) was larger than the hydrogenated film. They explained this contradiction by postulating the existence of two kinds of defects having different electron capture cross-sections. On the other hand, we have previously reported (Yang et al. 1994) that cells with high hydrogen dilution showed better performance both in the degraded and the initial states than that prepared with low hydrogen dilution, while defect density from CPM measurement showed no difference between them.

We have focused on deuterated amorphous silicon (a-Si:D) alloys deposited with deuterium dilution, which is a totally different regime from what was previously studied. We present here results on deuterated and hydrogenated a-Si alloy solar cells where intrinsic layers were deposited by using the same gas flow rates at the same deposition rate and show reduced light-induced degradation in the deuterated cells. We also present the similarity of hydrogen (deuterium) effusion results between heavily diluted a-Si:H alloy and normally diluted a-Si:D alloy. Possible explanations are discussed.

Experimental

Single-junction *p-i-n* solar cells were grown by the rf glow discharge technique on stainless steel substrates with predeposited silver-zinc oxide back reflector. The intrinsic layers were grown using the following gas mixtures: SiH_4+H_2, SiD_4+D_2, SiH_4+D_2, and SiD_4+H_2. The deposition temperature range investigated was between 150-300 °C. Except for one experiment where the doped layers also used deuterated gases, hydrogenated doped layers prepared under the same conditions were used for all the experiments. Light soaking at 50 °C under one-sun conditions was carried out on pairs of cells in which the intrinsic layer deposition parameters were similar except for the substitution of hydrogen by deuterium. In addition to the measurement of cell parameters in the initial and light-degraded states, the bonding and also the quantity of hydrogen/deuterium in the material were investigated using hydrogen/deuterium effusion, infrared, and secondary ion mass spectroscopy (SIMS) studies. The intrinsic alloy films were deposited on crystalline silicon wafers or bare stainless steel for these experiments.

Results and Discussion

Table VI shows the performance of a set of three solar cells in which the intrinsic layers were deposited at a substrate temperature of 200 °C. Sample 5742 uses deuterated material for all the layers (both doped and intrinsic), sample 5622 uses deuterated gas mixture only for the intrinsic layer, and sample 5752 has hydrogenated alloys for all the layers. The thicknesses of the three cells were identical. It is apparent from Table VI that the degradation in efficiency for the all-deuterated cell is similar to that of the cell where only the intrinsic layer is deuterated. Both the cells show lower degradation than the hydrogenated cell. The fill factor (FF) in the light-soaked state for the deuterated cells is higher than that of the hydrogenated cell. This indicates superior stability of the deuterated material. Table VI also shows a higher open-circuit voltage (V_{oc}) and lower short-circuit current density (J_{sc}) for the deuterated cell (5622) as compared to the hydrogenated cell (5752). Quantum efficiency versus wavelength data of both cells are shown in Fig. 1. It reveals that short wavelength (λ<500 nm) response of the two cells is similar, while the long wavelength (λ>500 nm) response accounts for the 2 mA/cm^2 difference in photocurrent. This indicates that the deuterated cell has a wider bandgap than the hydrogenated cell. Our preliminary measurement of deuterium/hydrogen in the films shows the deuterium content in the deuterated material to be higher than the hydrogen content in the hydrogenated material. This probably explains the change in the bandgap leading to the differences in V_{oc} and J_{sc}. We also find that the degradation in V_{oc} is much lower for the deuterated cell and is absent in the all-deuterated cell. Since the degradation of V_{oc} is believed to be caused both by the bulk and the interface, further investigation of this phenomenon may give us a better understanding of the relative importance of the two factors.

Table VI. **Initial and Light-soaked J-V Characteristics for *p i n* Cells Prepared with Different Gas Mixtures at the Same Gas Flow Rates and the Same Deposition Rate.**

Sample	Thickness (nm)	Temperature (°C)	Gas Mixture	Light-Soaked (hours)	Jsc (mA/cm^2)	Voc (V)	FF	Efficiency (%)
5742	310	200	*p,i,n*-layer:	0	13.72	0.977	0.678	9.09
			SiD_4+D_2	1010	13.30	0.977	0.632	8.21
				degradation (%)	3.1	0	6.8	9.7
5622	310	200	*p,n*-layer:	0	13.17	1.018	0.704	9.44
			SiH_4+H_2	1010	12.91	1.005	0.655	8.50
			i-layer:					
			SiD_4+D_2	degradation (%)	2.0	1.3	7.0	10.0
5752	310	200	*p,i,n*-layer:	0	15.13	0.968	0.676	9.90
			SiH_4+H_2	1010	14.46	0.930	0.607	8.16
				degradation (%)	4.4	3.9	10.2	17.6

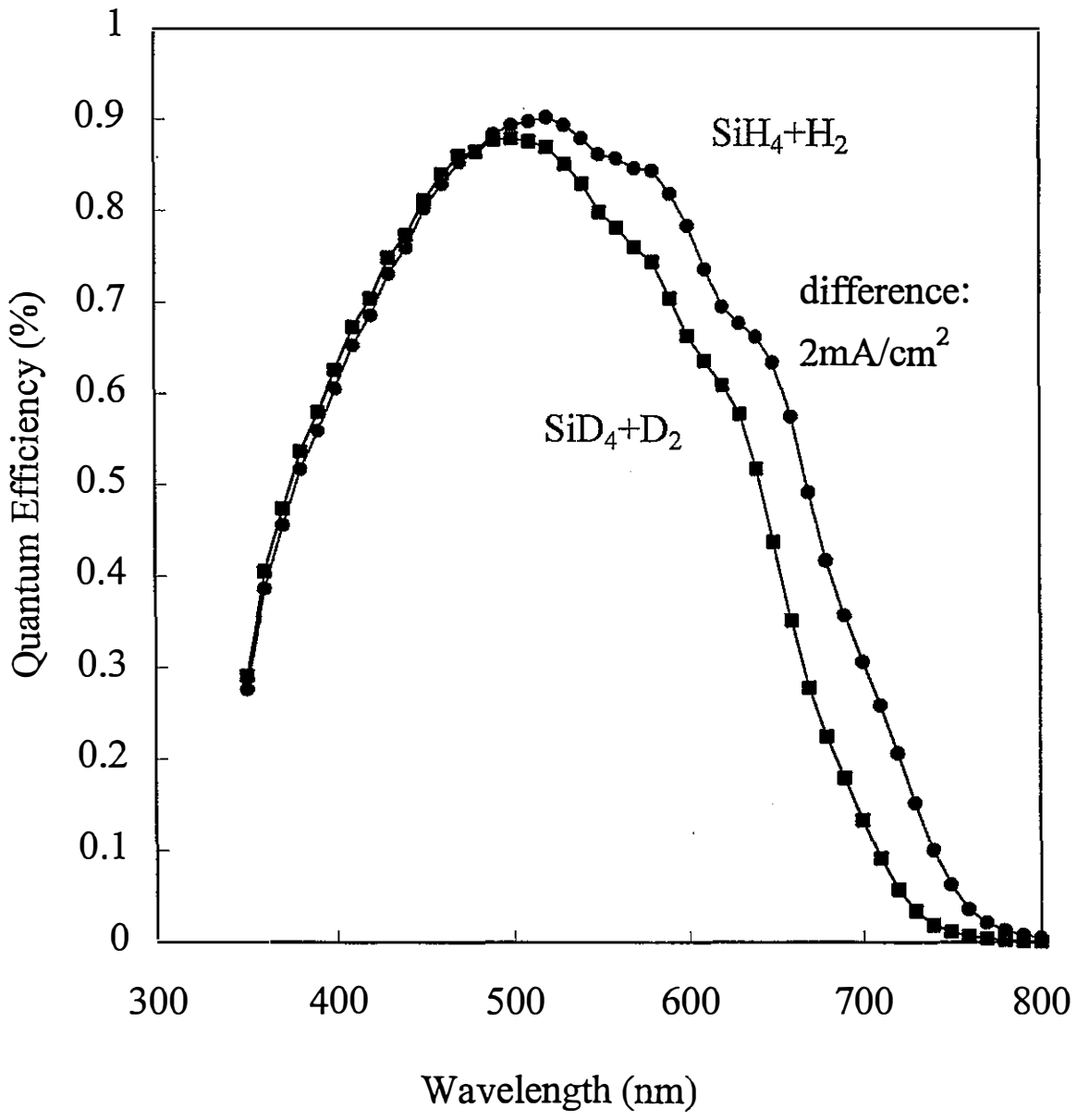

Figure 1. **Quantum efficiency versus wavelength data of hydrogenated and deuterated samples deposited with the same gas flow rates at the same deposition rate.**

In order to investigate if it is necessary to replace hydrogen completely to improve stability, we have also investigated the degradation behavior of cells where the intrinsic layers were made from SiH_4+D_2 and SiD_4+H_2 mixtures. As can be seen from Table VII, the degradation behavior is similar to cells made from SiH_4+H_2, while we have confirmed fairly high deuterium content in both the films by infrared absorption measurement. This result shows that improved stability in a-Si:D cell does not originate from simple replacement of hydrogen with deuterium. The reason why total elimination of hydrogen from the gas mixtures used for depositing the intrinsic layer is necessary for improving stability is not clear, but it is possible that some kind of structural change occurs in the film, and deuterium assists it better than hydrogen. We have also carried out experiments on cells in which the intrinsic layers are deposited at temperatures up to 300 °C and find the same trend in degradation, namely, the deuterated cells degrade less than the hydrogenated cells.

Table VII. Initial and Light-soaked J-V Characteristics for *p i n* Cells Prepared with SiH_4+D_2 and SiD_4+H_2 Gas Mixtures.

Sample	Thickness (nm)	Temperature (°C)	Gas Mixture	Light-Soaked (hours)	Jsc (mA/cm^2)	Voc (V)	FF	Efficiency (%)
5744	310	200	*p,n*-layer:	0	15.15	0.975	0.697	10.3
			SiH_4+H_2	1000	14.43	0.938	0.610	8.3
			i-layer:					
			SiH_4+D_2	degradation (%)	4.8	3.8	12.5	19.8
5818	310	200	*p,n*-layer:	0	14.35	1.004	0.665	9.6
			SiH_4+H_2	1000	13.23	0.980	0.602	7.8
			i-layer:					
			SiD_4+H_2	degradation (%)	7.7	2.4	9.5	18.5

Although the deuterated cells degrade less than their hydrogenated counterparts, degradation is not totally eliminated and the stabilized efficiency was not improved. SIMS analysis on our deuterated samples reveals hydrogen content to be about 10^{20}/cc. Since the metastable defect density is less than 10^{17}/cc, we can not rule out the possibility that the presence of this substantial amount of hydrogen may be responsible for the light-induced degradation. We do not know yet the source of the hydrogen contamination. The deuterated gases contain less than 10 ppm hydrogen. It is possible that the hydrogen is coming from the deposition chamber walls which are coated with hydrogenated alloys. Efforts are under way to eliminate the hydrogen contamination.

A plausible explanation for the hot electron degradation in transistors was provided (Lyding et al. 1996) in terms of the electron population of the Si-H antibonding states, resulting in a force that accelerates the hydrogen away from the silicon surface. That acceleration, of course, is diminished for deuterium because of its higher mass, giving rise to the lower degradation. While one can not rule out the population of the antibonding states of Si-H (D) by photogenerated electrons, the high value of the energy of such states (~5 eV above conduction band) makes the occupation probability low. A similar mechanism for improved stability is, therefore, less obvious. Hydrogen/deuterium effusion studies (Fig. 2) show that there is a

narrow peak at a lower temperature (~400 °C) in the deuterated material, whereas the corresponding peak does not exist in the hydrogenated material. The difference of this effusion spectra suggests that the structure of the two materials is different. It is interesting to point out that similar effusion at low temperature has also been observed in hydrogenated material grown with heavy hydrogen dilution at the lower deposition rate. (Xu et al. 1994). The hydrogen effusion measurement of the hydrogenated films depending on hydrogen dilution and deposition rates is shown in Fig 3. The peak at the lower temperature (~400 °C) does not exist for the film with normal hydrogen dilution and normal deposition rate, but the peak position is shifted to a lower temperature for the film with higher hydrogen dilution and normal deposition rate and the sharp peak at about 400 °C appears at the film with heavy hydrogen dilution and lower deposition rate. Films grown with heavy hydrogen dilution at the lower deposition rate have been found to have more oriented microstructures and low density of isotropic nanovoids as measured by small-angle X-ray scattering (SAXS). It has been speculated that this material is characterized by a more ordered microstructure which also leads to improved stability. The similarity in the effusion characteristics of the deuterated and the hydrogenated alloys deposited with heavy hydrogen dilution therefore indicates that the improved stability of the deuterated cells is also related to improved microstructure. The best stabilized fill factor for the deuterated cell with an *i*-layer thickness of 310 nm is 0.655. The corresponding value obtained for a hydrogenated cell grown with heavy hydrogen dilution and of 270 nm thickness is 0.63. The deuterated cell thus appears to have better stable FF than the best hydrogenated cell even though it is slightly thicker. A somewhat similar result about higher FF in a degraded deuterated cell was reported by Nevin et al. (Nevin et al. 1991). But the film structure, which we regard as very important, in their material must be quite different from ours because the degradation of their cells is very high. Also McElheny et al. (McElheny et al. 1991) reported that the deuterium effusion was greater at temperatures below 400 °C than hydrogen effusion, but their film structure is also different from ours because the effusion spectrum does not show any sharp peak and is only slightly different from the hydrogenated film.

We have also prepared a highly diluted hydrogenated cell by increasing the rf power to match the deposition rate of the deuterated cell. The initial and degraded characteristics of both cells are listed in Table VIII. Although we can not compare the characteristics directly because of the different thicknesses, the degradation of hydrogenated cell (6251) is higher even though its thickness is thinner. This result also agrees with hydrogen effusion data shown in Fig 3, where we find that the effusion spectra of the two films are quite different, suggesting that the film structures are also different. Although the reason why deuterium produces stable microstructure more easily than hydrogen is not clear, it is possible that deuterium with a higher mass impinges on the growing surface with a higher energy, forming a denser silicon network structure thus relaxing film stress. On the other hand, it is interesting to point out that the J_{sc} in hydrogenated cell is higher than the deuterated one even though hydrogenated cell has a smaller thickness and similar V_{oc}. We also observed a higher stable efficiency in hydrogenated cell, mainly due to its higher J_{sc}.

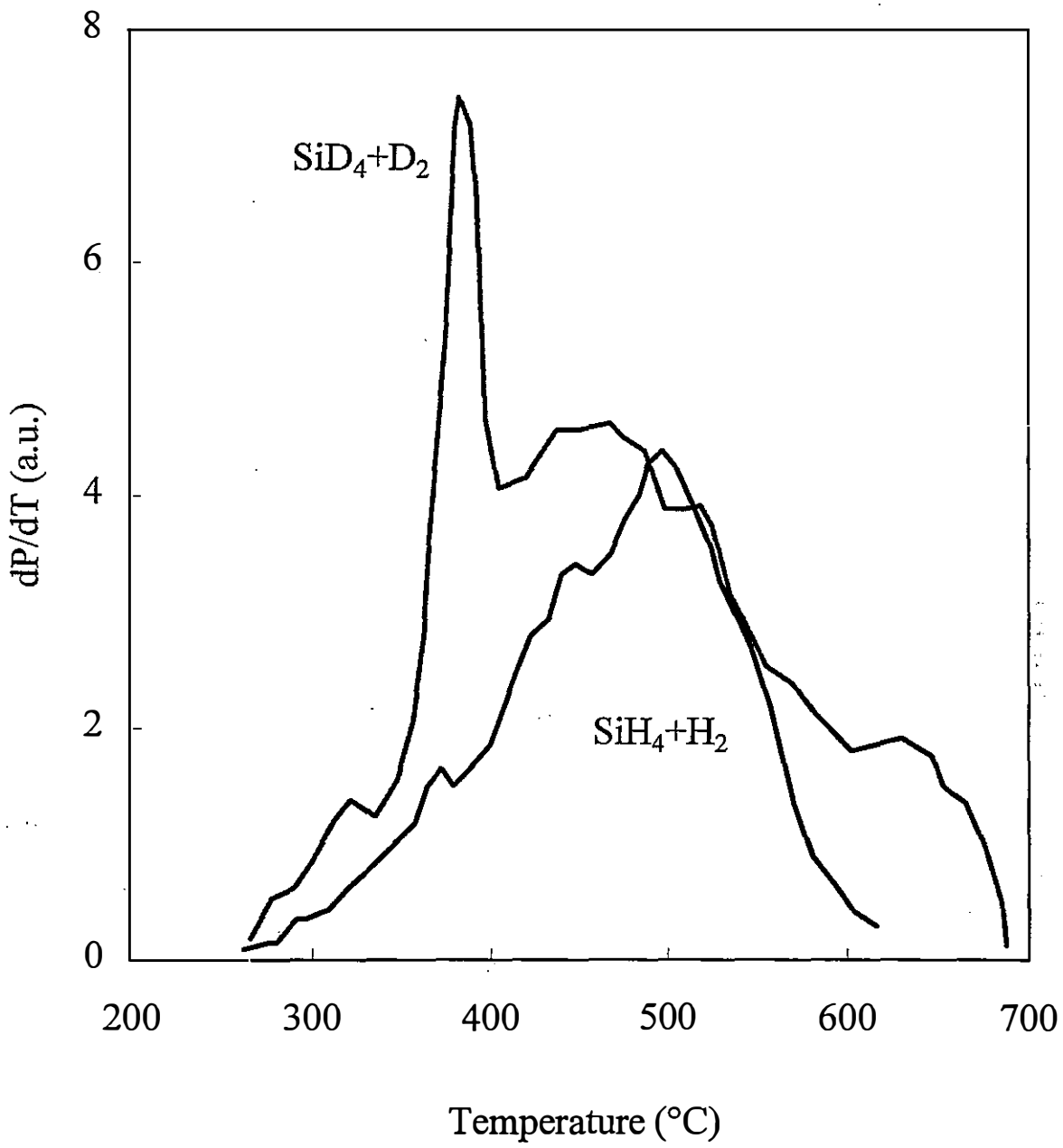

Figure 2. **Hydrogen (deuterium) effusion spectra from hydrogenated (deuterated) samples deposited by the same gas flow rate at the same deposition rate.**

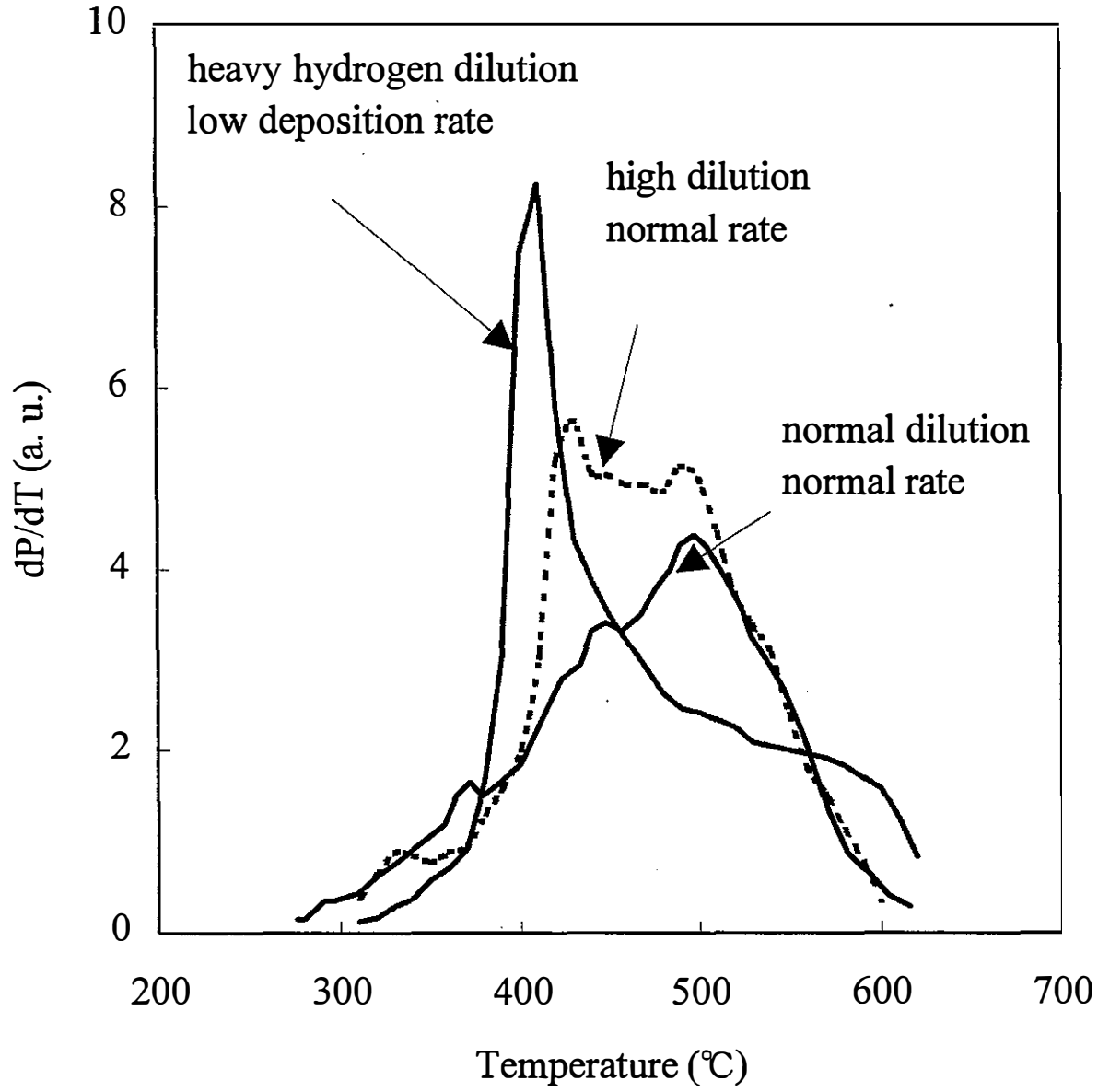

Figure 3. **Hydrogen effusion spectra from hydrogenated samples.**

Table VIII. Initial and Light-soaked J-V Characteristics for *p i n* Cells Prepared with SiD_4+D_2 and Highly Diluted SiH_4+H_2 Gas Mixtures at the Same Deposition Rate.

Sample	Thickness (nm)	Dilution D_2 (H_2)	Gas Mixture	Light-Soaked (hours)	Jsc (mA/cm^2)	Voc (V)	FF	Efficiency (%)
5622	310	normal	*p,n*-layer:	0	13.17	1.018	0.704	9.44
			SiH_4+H_2	1010	12.91	1.005	0.655	8.50
			i-layer:					
			SiD_4+D_2	degradation (%)	2.0	1.3	7.0	10.0
6251	230	high	*p,i,n*-layer:	0	14.69	1.012	0.707	10.51
			SiH_4+H_2	1010	13.82	0.980	0.646	8.75
				degradation (%)	5.9	3.2	8.6	16.7

The correlation between effusion at low temperature and stability of both hydrogenated and deuterated alloys strongly indicates that microstructure of the material plays a key role in improving the stability. Based on electron microscope and Raman studies, we have now found more direct evidences about the structural change related with film stability against light-exposure. The results will be published elsewhere. It is well-known that hydrogen etches the growing surface and, in the extreme case of high dilution and high applied power, can induce greater order. Our experiments on doped microcrystalline deuterated alloys presented earlier show that deuterium also behaves the same way. What is interesting, however, is the fact that in a very limited number of experiments, the deuterated cells show higher stabilized fill factor than the hydrogenated cells in spite of the wealth of experimentation done on the latter. This leads to the possibility of obtaining even better stability with the deuterated alloy as our understanding is further enhanced. It is also interesting that deuterium seems to produce this kind of microstructure at a higher deposition rate than hydrogen. Further understanding of this mechanism will help to develop deposition processes for production in which high deposition rate is desirable.

Section 5

Status of Component Cells for High Efficiency Triple-junction Solar Cells

Introduction

To achieve high efficiency triple-junction cells, several key issues need to be addressed. These include high quality (1) back reflectors, (2) top, middle, and bottom component cells, (3) "tunnel" junctions, (4) transparent conducting oxide, and (5) cell matching. This section discusses the status of component cells, Section 6 will address tunnel junction, transparent conducting oxide, and cell matching, and back reflector is within the scope of another NREL subcontract and will be reported separately.

Status of Component Cells

We should first mention that for the design of the component cells, our goal is to obtain high efficiency triple-junction cells having a J_{sc} of ≥8 mA/cm^2. This implies that each component cell should produce at least 8 mA/cm^2. Since the top and middle cells in a triple-junction configuration do not receive much reflected light, we deposited the top cell onto bare stainless steel substrates without any back reflector and the middle cell onto Cr coated textured back reflectors for evaluation.

For the top cell, we used a-Si alloy in the intrinsic layer made with high hydrogen dilution to improve the quality of the material. A microcrystalline *p* layer is used to enhance the built-in potential, reduce the optical loss, and improve the cell performance. The J-V characteristic of such a top cell exhibits an initial V_{oc} of 1.038 V, J_{sc} of 10.13 mA/cm^2, FF of 0.740, and efficiency of 7.78%. This is the highest efficiency value reported for a top cell for triple-junction applications and represents a significant improvement over Phase II status of 6.2%. The J_{sc} value of 10.13 mA/cm^2 is certainly sufficient for the top cell requirement.

For the middle cell, we used a high hydrogen diluted gas mixture of Si_2H_6 and GeH_4 in the *i* layer. The cell was deposited onto a standard back reflector but coated with Cr to reflect the fact that the middle cell does not receive much reflection from the substrate. The initial J-V characteristic measured with AM1.5 through a 530 nm cut-on filter shows V_{oc} = 0.753 V, J_{sc} = 9.30 mA/cm^2, FF = 0.687, and P_{max} = 4.81 mW/cm^2. The 530 nm filter was used to simulate the middle cell's insolation in a triple-junction structure. The current density of 9.3 mA/cm^2 measured through a 530 nm filter is appropriate for the middle cell in a triple-junction structure.

The bottom cell was deposited onto a textured Ag/ZnO back reflector and incorporated an a-SiGe alloy *i* layer made using high hydrogen dilution and band gap profiling techniques. The initial J-V characteristic measured with AM1.5 through a 630 nm cut-on filter shows V_{oc} = 0.631 V, J_{sc} = 12.2 mA/cm^2, FF = 0.671, and P_{max} = 5.17 mW/cm^2. The initial power output of 5.17 mW/cm^2 is the highest reported to date and represents a significant improvement over Phase II status of 4.64 mW/cm^2. The quantum efficiency versus wavelength plot is shown in Fig. 4. It is noted that at 850 nm, the quantum efficiency is 45%, indicative of a high quality back reflector. Table IX summarizes the initial characteristics of the component cells.

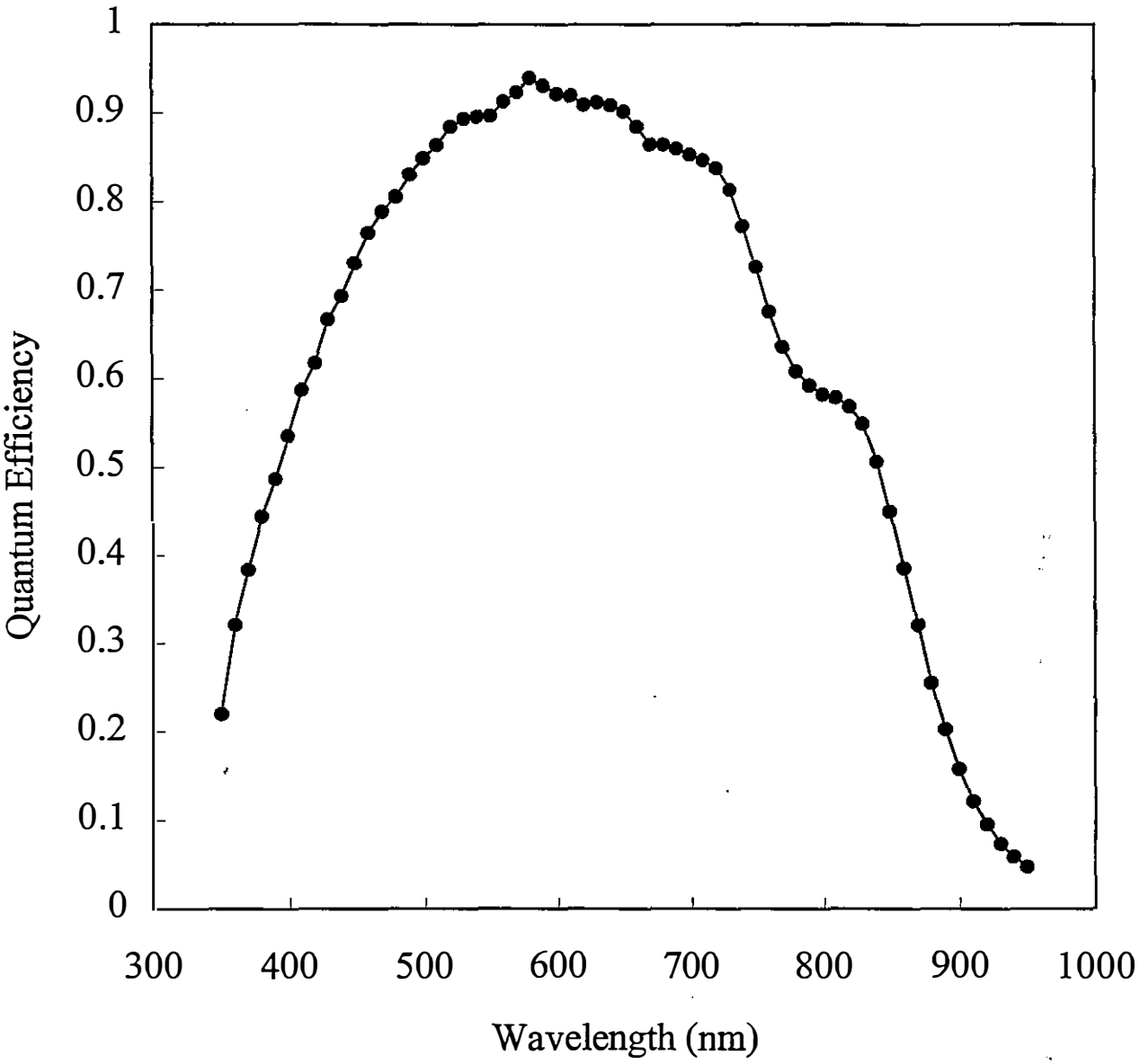

Figure 4. **Quantum efficiency of an a-SIGe alloy bottom cell on Ag/ZnO back reflector showing a 45% value at 850 nm.**

Table IX. Initial J-V Characteristics of the Top, Middle, and Bottom Component Cells.

Component Cell	J_{sc} (mA/cm^2)	V_{oc} (V)	FF	P_{max} (mW/cm^2)
Top[ad]	10.13	1.038	0.740	7.78
Middle[be]	9.30	0.753	0.687	4.81
Bottom[cf]	12.2	0.631	0.671	5.17

[a] deposited onto bare stainless steel without back reflector
[b] deposited onto textured back reflector coated with Cr
[c] deposited onto textured Ag/ZnO back reflector
[d] measured under AM1.5 illumination
[e] measured under AM1.5 illumination with a 530 nm cut-on filter
[f] measured under AM1.5 illumination with a 630 nm cut-on filter

Stability of Component Cells

We used a metal-halide lamp with the intensity adjusted to one sun to study the stability of the component cells. For J-V measurements, the top cell was measured with AM1.5 illumination, while the middle and bottom cells were measured through 530 and 630 nm cut-on filters, respectively. All the component cells were light-soaked in the open-circuit mode and the temperature was maintained at 50 °C.

In general, the component cells show substantial saturation after ~200 hours of light-soaking, typical of high quality amorphous silicon alloy solar cells. Table X compares stabilized active-area cell efficiency for the top, middle, and bottom component cells to date and at the beginning of the program. One can easily note that significant progress has been made in the stabilized performance and should be reflected in the performance of the triple-junction structures to be discussed in the next section.

In order to obtain a 15% stable module efficiency, Guha et al. (Guha et al. 1994) has estimated that a 16% stabilized small-area cell efficiency is necessary. Table X also lists values estimated for reaching the 16% goal. One can see from Table X that J_{sc} values have substantially surpassed the goal while improvement needs to be made on V_{oc} and FF. This can only be met by innovative material research and device design with continued focused effort. This is particularly true for a-SiGe alloy material.

Table X. Stabilized Active-area Component Cell Status at United Solar at the Beginning of the Program and Present.

Component Cell	Status	J_{sc} (mA/cm^2)	V_{oc} (V)	FF	P_{max} (mW/cm^2)
Top[a]	beginning[d]	7.2	0.98	0.71	5.0
	present[e]	8.78	0.953	0.709	5.93
	goal	8.2	1.10	0.75	6.8
Middle[b]	beginning[d]	6.9	0.74	0.57	2.9
	present[d]	8.92	0.717	0.587	3.75
	goal	8.4	0.89	0.70	5.2
Bottom[c]	beginning[f]	7.7	0.65	0.56	2.8
	present[f]	11.12	0.609	0.622	4.21
	goal	8.6	0.68	0.68	4.0

[a] measured under AM1.5
[b] measured under AM1.5 with a λ>530 nm filter
[c] measured under AM1.5 with a λ>630 nm filter
[d] deposited onto a textured substrate coated with Cr
[e] deposited onto a bare ss substrate
[f] deposited onto a textured Ag/ZnO substrate

Achieving Highest Stable a-Si Alloy Single-junction Cell Efficiency

The highest stable single-junction a-Si alloy solar cell efficiency of 8.9% was reported recently by Kameda et al. (Kameda et al. 1996). Since we have shown that hydrogen dilution improves the cell stability, we have recently conducted light-soaking experiments in single-junction a-Si alloy *p i n* solar cells on Ag/ZnO back reflector. After 1500 hours of one-sun light soaking at 50 °C, the degraded efficiency is 9.2%, establishing a new world record for this structure. Table XI lists the initial and degraded J-V characteristics of the cells.

Table XI. **Initial and Degraded (1500 hours) J-V Characteristics of a-Si Alloy Single-junction Cell with High Hydrogen Dilution and Deposited on Ag/ZnO Back Reflector.**

Sample	Status	J_{sc} (mA/cm^2)	V_{oc} (V)	FF	P_{max} (mW/cm^2)
8934 #33	Initial	15.6	0.983	0.692	10.6
	Degraded (1500 hours)	15.0	0.949	0.645	9.2
	Degradation (%)	3.8	3.5	6.8	13.4

Section 6

Achievement and Analysis of Record 14.6% Initial and 13% Stable Active-area Efficiencies for Triple-junction Solar Cells

Introduction

As discussed in Section 5, significant improvement has been made in the performance of component cells during Phase III of the program. In addition to incorporating the component cell results into the triple-junction structure, component cell current mismatch and tunnel junction characteristics need to be optimized. At the end of Phase II of this program, we reported the achievement of an 11.8% stable active-area cell efficiency. In this section, we discuss the three key improvements that enabled us to achieve record 14.6% initial and 13.0% stable active-area cell efficiencies.

Experimental Results and Discussion

Figure 5 shows a schematic diagram of the triple-junction structure. The top intrinsic (*i*) layer uses wide bandgap a-Si alloy for absorbing the blue photons, while the middle and bottom *i* layers incorporate intermediate and narrow bandgap amorphous silicon-germanium (a-SiGe) alloys for absorbing the green and red photons, respectively. A textured silver/zinc-oxide back reflector is used to facilitate light trapping (Ross et al. 1987). The red photons that reach the back surface are scattered back at an oblique angle so as to enhance the optical path and provide additional absorption. The top contact uses indium-tin-oxide (ITO) which also serves as an antireflection coating. Finally, a metal grid is deposited on top of ITO for collecting current.

All the three *i* layers use high hydrogen dilution during film growth to obtain superior quality (Yang et al. 1994), and the middle and bottom a-SiGe *i* layers employ bandgap profiling for better carrier collection (Guha et al. 1989). Microcrystalline *p* layers with high conductivity and low optical absorption (Guha et al. 1986) are used as the window layer as well as in the tunnel junctions.

Using the above approach, along with an appropriate current mismatching cell design, we recently obtained a triple-junction cell with 13.2% initial and 11.8% stable efficiencies (Yang et al. 1996). Figure 6 plots the initial quantum efficiency data for this device. It is noted that the total photocurrent generated in the triple stack is ~25 mA/cm^2.

A careful analysis of Fig. 6 reveals that one can possibly further improve the spectrum response in three areas: (a) the red response in the long wavelength (λ>800 mn) region, (b) the response associated with the absorption of the tunnel junction between the top and the middle cells in λ~500-600 nm region, and (c) the blue response in the short wavelength (λ<450 mn) region.

The Red Response

One way to enhance the red response, hence increasing the triple-cell current with desired current mismatch, is to increase the germanium content in the bottom cell. This, however, often results in a poorer material quality and deteriorates the cell performance. Using high hydrogen dilution during film growth and incorporating proper bandgap profiling, we have improved the bottom component cell with

Figure 5. **Schematic diagram of a triple-junction cell structure.**

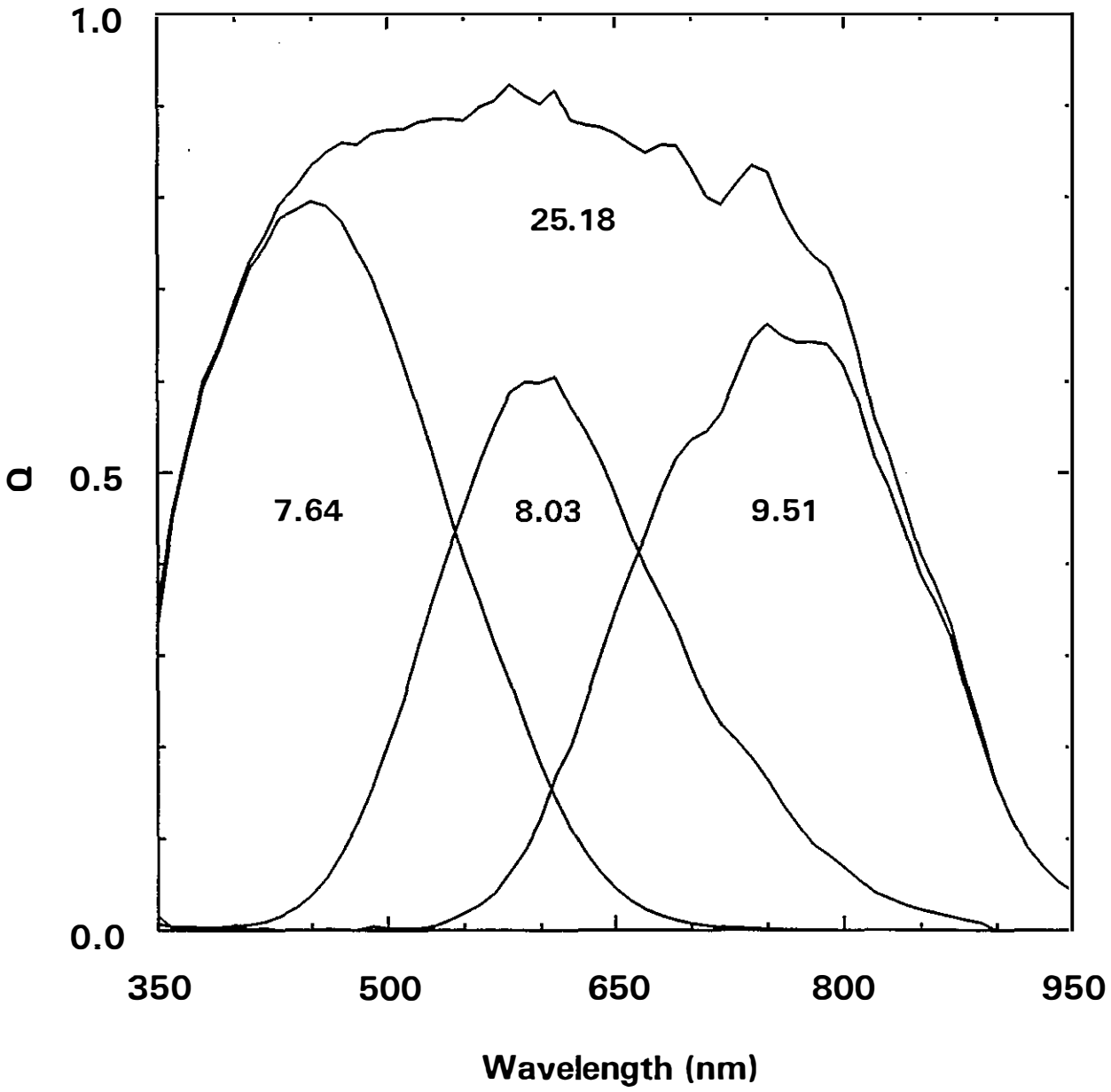

Figure 6. Initial quantum efficiency of the previous best triple cell.

an enhanced red performance. Table XII compares the performance of the previous and recent bottom cells measured under AM1.5 illumination through a λ>630 nm red filter. It is readily observed that the recent cell has a higher red current and improved output power. The higher V_{oc} and FF demonstrate the benefit of proper hydrogen dilution and bandgap profiling. Since the previous cell was used to obtain the 11.8% stable device, the improved cell should set a good foundation for a triple-junction structure. The improved bottom cell under AM1.5 illumination shows J_{sc} = 24.4 mA/cm^2, V_{oc} = 0.662 V, FF = 0.643, and an AM1.5 efficiency of 10.4%. The quantum efficiency data for this device reveal that at 850 nm the collection is 45%, a significant improvement over the 35% value reported for the previous bottom cell (Yang et al. 1996).

Table XII. Initial J-V Characteristics of Previous and Recent Bottom a-SiGe Cells Measured under AM1.5 Illumination with a λ>630 nm Filter.

	J_{sc} (mA/cm^2)	V_{oc} (V)	FF	P_{max} (mW/cm^2)
Previous	11.9	0.611	0.634	4.6
Recent	12.2	0.631	0.671	5.2

The Tunnel Junction

There are two tunnel junctions in the triple structure (see Fig. 5). One is p_2n_3 between the top and the middle cells, and the other is p_1n_2 between the middle and the bottom cells. These tunnel junctions, while essential in the triple-cell operation, result in optical and electrical losses. Any reduction in their optical absorption or electrical resistance, for example, by using microcrystalline doped layers, should give rise to a better cell performance. In our earlier triple-junction cells, we have used microcrystalline *p* layer but amorphous *n* layer in the tunnel junctions.

Since the p_2n_3 top tunnel junction is closer to where light enters the device than the p_1n_2 junction, any improvement in the top tunnel junction is expected to result in a larger improvement in the cell performance. To evaluate the top tunnel junction, we first studied two a-Si/a-Si double-junction cells. The only difference between the two cells is that one uses an amorphous *n* layer while the other uses a microcrystalline *n* layer in the tunnel junction. To our surprise, we find that the V_{oc} value for the tandem cell having a microcrystalline *pn* junction is much lower (V_{oc}=1.657 V) than the corresponding one (V_{oc}=1.804 V). We attribute the lowering of V_{oc} to the following two reasons: (a) The microcrystalline *n* layer may have much lower bandgap than the amorphous *i* layer, and the band edge discontinuity (Xu et al. 1995) may cause the lowering of V_{oc}. (b) The deposition conditions for microcrystalline material generally require high rf power and high hydrogen dilution (Guha et al. 1986). These conditions can cause the intermixing of the dopants in the thin doped layers, thus lowering the V_{oc}.

We have developed novel buffer layers and inserted them between the microcrystalline *p* and *n* layers, and between the microcrystalline *n* and amorphous *i* layers. We then compared the a-Si/a-Si double-junction performance by using a conventional amorphous *n* layer, and a microcrystalline *n* layer sandwiched between buffer layers in the tunnel junction. We have taken care to deposit the companion pairs onto the same back reflector; the pairs also have the same ITO deposited onto them. The results are listed in Table XIII. It is observed that the microcrystalline *pn* multilayered structure gives rise to cells with higher J_{sc}, V_{oc}, FF, total current, and efficiency. The higher total current and lower series resistance demonstrate the improvement due to the new tunnel junction structure.

Table XIII. Characteristics of a-Si/a-Si Double Junctions with Different Tunnel Junction Structures.

Tunnel Junction Structures	J_{sc} (mA/cm^2)	V_{oc} (V)	FF	η (%)	Qtop/Qbtm (mA/cm^2)	Qtotal (mA/cm^2)	R_s (Ω cm^2)
microcrystalline *p* amorphous *n*	7.80	1.901	0.752	11.15	7.97/7.80	15.77	15.0
microcrystalline *p* multilayered *n*	8.06	1.919	0.766	11.85	8.06/8.28	16.34	14.3

The Blue Response

As mentioned earlier, the top conducting oxide serves as the top contact (see Fig. 5) as well as an antireflecting coating. If one can reduce the absorption in ITO without sacrificing its conductivity, one can gain in photocurrent. This will benefit the entire triple stack with the top cell receiving the most advantage. We have reoptimized the ITO deposition conditions by adjusting the oxygen partial pressure and obtained a higher ITO transmission. A top cell with the improved ITO shows a J_{sc} value ~0.5 mA/cm^2 higher than that obtained with previous ITO. The higher current is achieved without increasing the *i* layer thickness, which is certainly desirable from the stability point of view. A J_{sc} value of ~8.5 mA/cm^2 is also suitable for the top cell of a triple structure with the improved bottom component cell.

The Triple-junction Cell

Incorporating the improvements described above, we then proceeded to make triple-junction cells with microcrystalline *p* and multilayered *n* structure in both tunnel junctions. Several triple cells with initial efficiencies exceeding 14% were obtained. The highest efficiency achieved is 14.6%, representing a 10% improvement over our previous record of 13.2% (Yang et al. 1996).

Figure 7 shows the J-V characteristic of the 14.6% triple-junction cell. Compared to our earlier best triple cell, J_{sc} is increased significantly from 7.64 to 8.57 mA/cm^2, while V_{oc} and FF have similar values. Quantum efficiency data shown in Fig. 8 reveal that the total photocurrent from the triple stack is 26.88 mA/cm^2, a significant increase from our earlier value of 25.18 mA/cm^2.

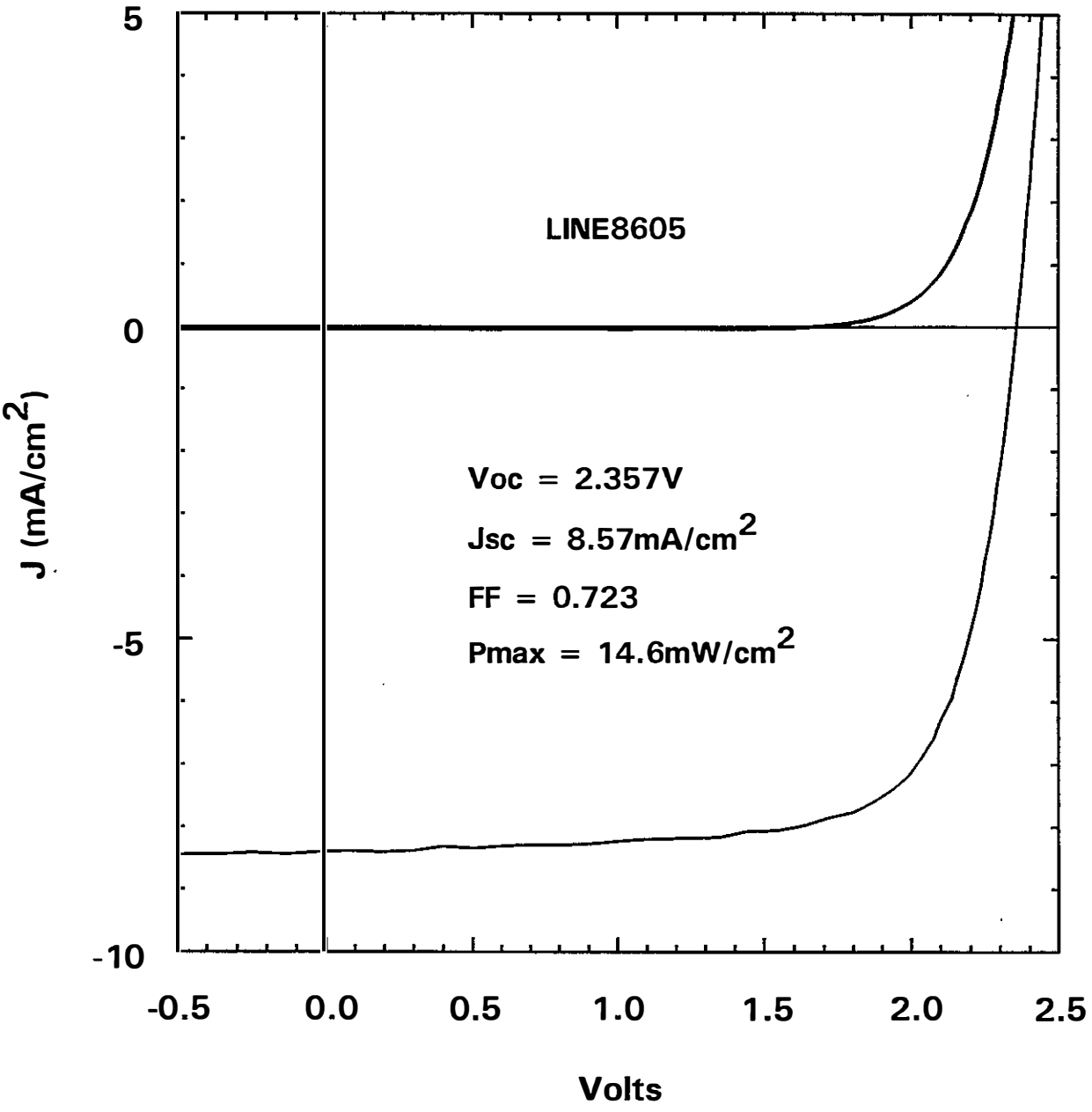

Figure 7. Initial J-V characteristic of the 14.6% triple-junction cell.

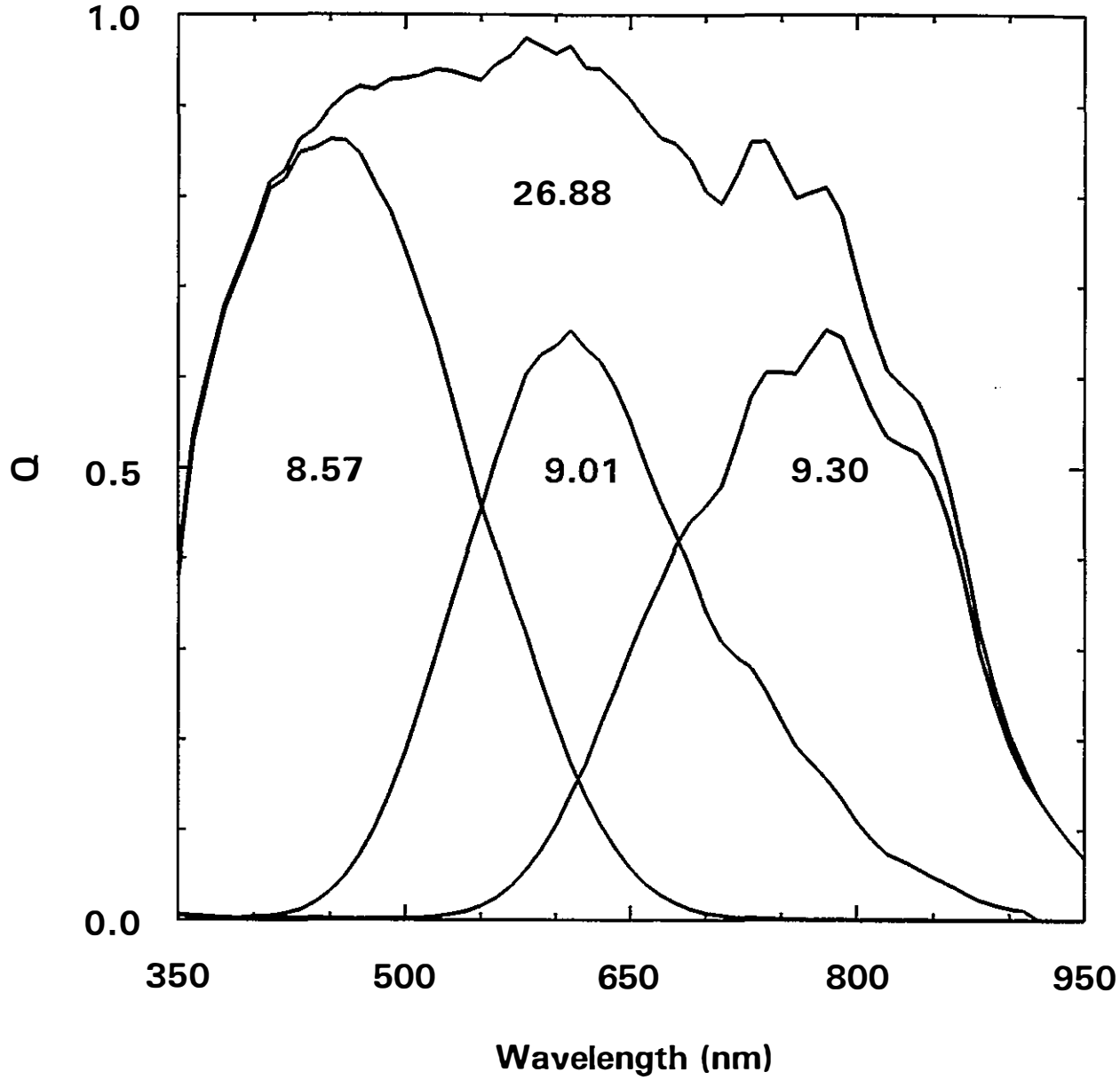

Figure 8. Quantum efficiency of the triple cell in Fig. 7.

Comparing Figs. 6 and 8, one can readily see that (a) the quantum efficiency for λ>800 nm is increased significantly due to the improvement in the red response; (b) the quantum efficiency for λ~500-600 nm region is improved due to the new tunnel junction structure; and (c) the overall quantum efficiency is enhanced, especially for the λ<450 nm region, due to the improvement in ITO. We indeed benefit from the three improvements discussed above.

Several devices were sent to NREL for triple-source measurement. Table XIV summarizes the data obtained at NREL and United Solar, demonstrating an excellent agreement between the two laboratories. It should be pointed out that the J_{sc} value at United Solar is based on quantum efficiency measurement. NREL measures the total area efficiency only; the active-area current density is obtained by subtracting the grid coverage from the total area.

Table XIV. Initial and Stable Triple Cell Efficiency (active area of ~0.25 cm^2) as Measured at United Solar and NREL.

Device L8605	V_{oc} (V)	I_{sc} (mA)	FF (%)	J_{sc} (total area) (mA/cm^2)	η (%)	J_{sc} (active area) (mA/cm^2)	η (%)	Measurement Laboratory
Initial	2.357		72.3			8.57	14.6	United Solar
Initial	2.357	2.104	74.39	7.721	13.5	8.28	14.5	NREL
Stable	2.294		68.4			8.27	13.0	United Solar
Stable	2.297	2.061	69.7	7.563	12.1	8.11	13.0	NREL

These devices were subsequently subjected to light soaking under one-sun, 50 °C, and open-circuit conditions. After ~300 hours of light soaking, their performance was substantially stabilized. The best stabilized efficiency after 1000 hours is 13.0%; it is again independently confirmed by NREL (Table XIV). This is the highest stable efficiency achieved for amorphous silicon alloy solar cells.

Analysis of High Efficiency Triple Cells

In order to evaluate the impact of the individual component cell on the performance of the high-efficiency device, we have analyzed the photovoltaic characteristics of the component cells made using the same parameters as those incorporated into the triple structure. The initial J-V characteristics measured under various illumination conditions are summarized in Table XV. The following observations are made for the initial performance:

1. The top cell exhibits the best fill factor. Therefore, it is desirable to design the triple structure using the top cell as the current-limiting cell, especially in the degraded state. Although the top cell is deposited onto a bare stainless steel substrate without any back reflector, it still receives some reflection from the substrate. This explains the somewhat smaller J_{sc} value in the triple configuration.

Table XV. Initial and Light-soaked J-V Characteristics of the Component and Triple-junction Cells at United Solar.

Cell	Status	J_{sc} (mA/cm^2)	V_{oc} (V)	FF	P_{max} (mW/cm^2)
top[d]	initial[a]	8.97	0.980	0.761	6.69
middle[e]	initial[b]	9.30	0.753	0.687	4.81
bottom[f]	initial[c]	12.2	0.631	0.671	5.17
triple[d]	initial[c]	8.57	2.357	0.723	14.6
top[d]	1994 stable[b]	7.3	0.97	0.72	5.1
	1997 stable[a]	8.78	0.953	0.709	5.93
middle[e]	1994 stable[b]	7.6	0.76	0.60	3.5
	1997 stable[b]	8.92	0.717	0.587	3.75
bottom[f]	1994 stable[c]	9.84	0.67	0.55	3.60
	1996 stable[c]	11.4	0.60	0.56	3.80
	1997 stable[c]	11.12	0.609	0.622	4.21
triple[d]	1995 stable[c]	6.87	2.38	0.68	11.1
	1996 stable[c]	7.49	2.283	0.692	11.8
	1997 stable[c]	8.27	2.294	0.684	13.0

a deposited on a bare stainless steel substrate
b deposited on a textured substrate coated with Cr
c deposited on textured Ag/ZnO back reflector
d measured under AM1.5 illumination
e measured under AM1.5 with a λ>530 nm filter
f measured under AM1.5 with a λ>630 nm filter

2. The photocurrent generated by the top, middle, and bottom component cells for the 14.6% triple cell are respectively 8.57, 9.01, and 9.30 mA/cm^2. The bottom component cell in Table XV shows 12.2 mA/cm^2 for J_{sc}, much higher than 9.30 mA/cm^2 obtained from the quantum efficiency measurement. The 630 nm filter used to evaluate the bottom cell may be insufficient for the narrow bandgap amorphous silicon-germanium bottom cell that we have recently developed. We need to use a longer wavelength filter so that the J_{sc} value will more appropriately simulate the operation of the bottom cell in a triple stack. However, to evaluate the progress in cell technology, the 630 nm filter is still used.

3. A simple arithmetic sum of the V_{oc} values of the component cells in the initial and light-soaked states give composite V_{oc} values within 1% of the corresponding triple-junction V_{oc} values.

4. Based on the above observations, one notices that in the triple-junction operation, J_{sc} is basically dictated by the top cell, V_{oc} is simply the sum of the individual V_{oc} values, and FF is governed by the top cell and the mismatch of the component cells. The initial triple-cell performance can be projected using the component cell characteristics.

To corroborate the performance of the triple cell after light soaking and the above analysis, we have carried out indoor light-soaking experiments using the same procedure as reported previously. The stable characteristics are tabulated in Table XV under 1997 values. The observations made for the initial states hold true for the degraded states as well. We have also listed in Table XV stabilized performance obtained at United Solar since the beginning of the Thin Film Partnership Program in 1994. The component cells in 1994 led to the achievement of 11.1% stable triple cell in 1995. The improvement in the bottom cell in 1996 as well as the current mismatch consideration resulted in the 11.8% stable triple-cell efficiency in 1996. The advances in the stabilized component cells, particularly the enhancement of J_{sc} resulted from improving the spectral response in the wavelength range of 300 to 1000 nm, help achieve the high efficiency.

Temperature Coefficient of High Efficiency Triple-junction Solar Cells

The three critical parameters that determine the efficiency of a solar cell, namely, open-circuit voltage, short-circuit current density and fill factor, all depend on the operating temperature. As the temperature increases, the open-circuit voltage decreases, the short-circuit current density increases, and the fill factor may increase or decrease depending on the design of the cell. For a triple-junction cell, the situation is more complex since the fill factor quite often is determined by that of the limiting cell and the degree of current mismatch among the different cells. It is, therefore, of interest to study the effect of current mismatch on the temperature coefficient of high efficiency triple-junction cells.

We have selected three devices with current matching conditions obtained from quantum efficiency measurements (Table XVI). It is noted from Table XVI that while the devices exhibit different component cell current distributions, their total current remains constant. For L9323, Q_{top}, Q_{middle} and Q_{bottom} have similar values; for L9329, Q_{top} and Q_{middle} have similar values, but Q_{bottom} is substantially larger; for L9330, Q_{middle} and Q_{bottom} have similar values, and Q_{top} is substantially smaller.

Table XVI. Component Cell Current Distribution for Three Triple-junction Solar Cells.

Device	Q_{top} (mA/cm^2)	Q_{middle} (mA/cm^2)	Q_{bottom} (mA/cm^2)	Q_{total} (mA/cm^2)
L9323	8.27	8.47	8.74	25.5
L9329	7.81	8.18	9.41	25.4
L9330	7.86	8.77	8.89	25.5

We measured the J-V characteristics for the three devices in the temperature range of 25 °C to 65 °C and plotted their characteristics in Figs. 9 and 10. From these two figures, we observe that the slope of efficiency versus temperature, i.e., the temperature coefficient, is similar for all three samples. In other words, the temperature coefficiency is rather insensitive to the current mismatch conditions. We plan to study the temperature coefficient of these devices in the light-soaked state. The experimental result will be useful in the component cell mismatch design for photovoltaic products.

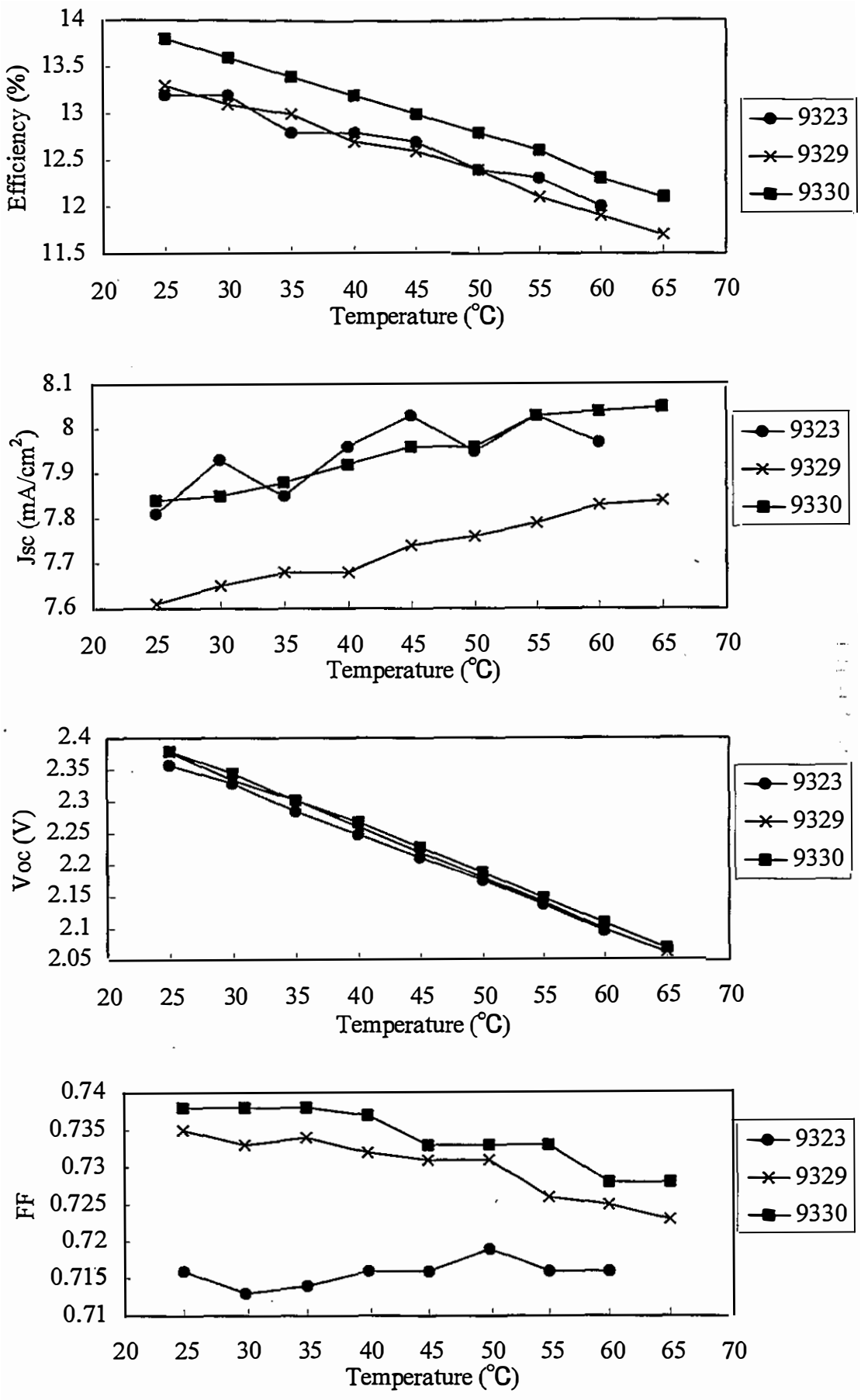

Figure 9. **Temperature dependence of Eff., J_{sc}, V_{oc}, and FF of samples L9323, L9329, and L9330.**

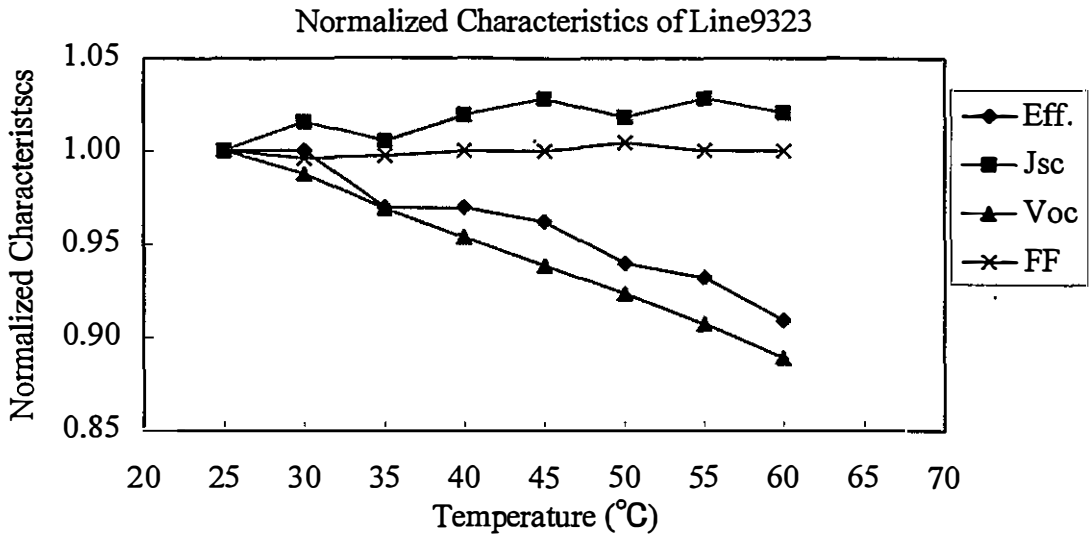

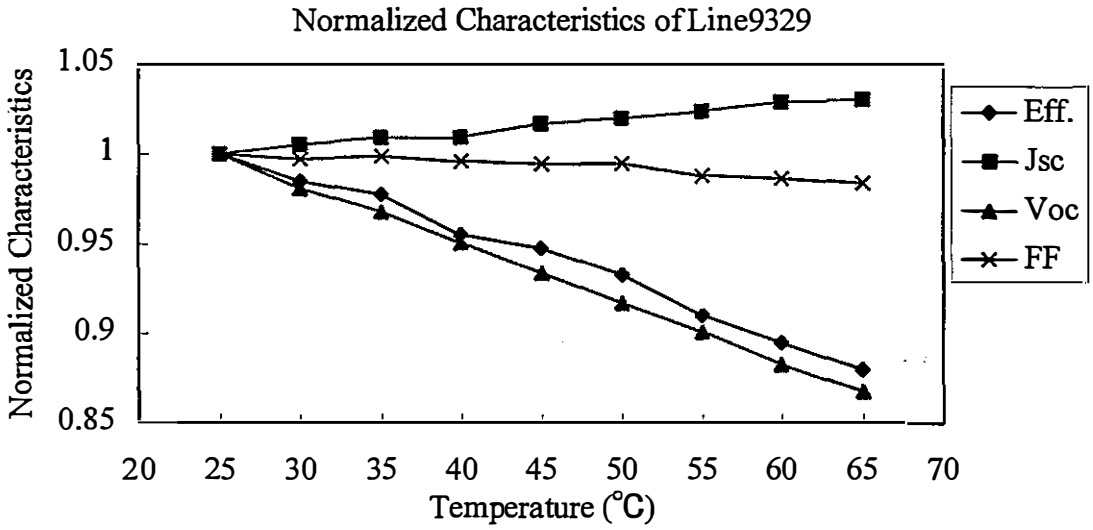

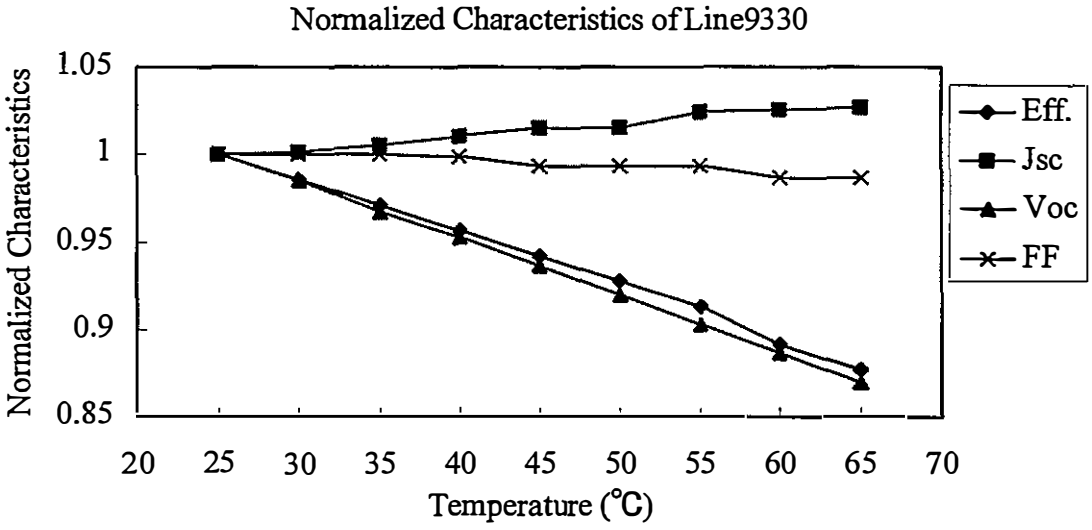

Figure 10. Temperature dependence of Eff., J_{sc}, V_{oc}, and FF of samples L9323, L9329, and L9330.

Section 7

Future Directions

Significant progress in stable efficiency of both component and triple cell structures has been shown during this program. The increase in efficiency has been achieved through a better understanding of the role of precursor gases and their effect on growth kinetics. Innovative device design to reduce tunnel junction losses has also played an important role. Our fundamental studies will continue, and we expect to see continuous improvements in efficiency through these efforts.

A major focus of the future programs will, however, be devoted toward the improvement of cell performance at higher deposition rates. The best cells are made at around 1 Å/s; to reduce capital cost for a given throughput, the production machines typically use deposition rates of around 3 Å/s. The higher deposition rates give rise to poorer efficiency. Improvement of efficiency for cells deposited at high rates will have a significant effect on product cost and acceptability. We shall investigate different deposition regimes to understand the plasma chemistry and growth kinetics at high rates so as to optimize cells at rates between 3-5 Å/s.

References

Gallagher, A.; Barzen, S.; Childs, M.; Laracuente, A. (1996). *Atomic-Scale Characterization of Hydrogenated Amorphous-Silicon Films and Devices.* NREL/SR-520-22565. Golden, CO: National Renewable Energy Laboratory. Work performed at National Institute of Standards and Technology, Boulder, Colorado.

Ganguly, G.; Suzuki, A.; Yamasaki, S.; Nomoto, K.; Matsuda, A. (1990). *J. Appl. Phys.*; Vol. 68, p. 2738.

Ganguly, G.; Yamasaki, S.; Matsuda, A. (1991). *Phil. Mag.;* Vol. B 63, p. 281.

Ganguly, G.; Matsuda, A. (1994). *Phys. Rev. B;* Vol. 49, p. 10986.

Guha, S.; Yang, J.; Czubatyj, W.; Hudgens, S.J.; Hack, M. (1983). *Appl. Phys. Lett.*; Vol. 42, p. 588.

Guha, S.; Yang, J.; Nath, P.; Hack, M. (1986). *Appl. Phys. Lett.*; Vol. 49, p. 218.

Guha, S.; Yang, J.; Pawlikiewicz, A.; Glatfelter, T.; Ross, R.; Ovshinsky, S.R. (1989). *Appl. Phys. Lett.;* Vol. 54, p. 2330.

Guha, S.; Yang, J.; Banerjee, A.; Glatfelter, T.; Hoffman, K.; Xu, X. (1994). *Solar Energy Materials and Solar Cells;* Vol. 34, pp. 329-337.

Kameda, M.; Sakai, S.; Isomura, M.; Sayama, K.; Hishikawa, Y.; Matsumi, S.; Haku, H.; Wakisaka, K.; Tanaka, M.; Kiyama, S.; Tsuda, S.; Nakano, S. (1996). *Conference Record of the 25th IEEE Photovoltaic Specialists Conference–1996*; p. 1059.

Lyding, J.W.; Hess, K.; Kizilyalli, C. (1996). *Appl. Phys. Lett.*; Vol. 68, p. 2526.

McElheny, P.J.; Suzuki, A.; Mashima, S.; Hasezaki, K.; Yamasaki, S.; Matsuda, A. (1991). *J. J. Appl. Phys.*; Vol. 30, p. L142.

Nevin, W.A.; Hamagishi, H.; Asaoka, K.; Nishio, H.; Tawada, Y. (1991). *Appl. Phys. Lett.*; Vol. 59, p. 3294.

Ross, R.; Mohr, R.; Fournier, J.; Yang, J. (1987). *Conference Record of the 19th IEEE Photovoltaic Specialists Conference–1987*; p. 327.

Wronski, C.R; Maley, N. (1991). *AIP Conference Proceedings 234-1991*; pp. 11-18.

Xu, X.; Yang, J.; Guha, S. (1994). *J. Non-cryst. Solids*; Vol. 198-200, p. 60.

Xu, X.; Yang, J.; Banerjee, A.; Guha, S.; Vasanth, J.; Wagner, S. (1995) *Appl. Phys. Lett.*; Vol. 67, p. 2323.

Yang, J.; Xu, X.; Guha, S. (1994). *Mat. Res. Soc. Symp. Proc.*; Vol. 336, p. 687.

Yang, J.; Banerjee, A.; Glatfelter, T.; Hoffman, K.; Xu, X.; Guha, S. (1994). *Conference Record of First World Conference on Photovoltaic Energy Conversion–1994*; p. 380.

Yang, J.; Xu, X.; Banerjee, A.; Guha, S. (1996). *Conference Record of the 25th IEEE Photovoltaic Specialists Conference–1996;* p. 1041.

REPORT DOCUMENTATION PAGE

Form Approved
OMB NO. 0704-0188

1. AGENCY USE ONLY (Leave blank)	2. REPORT DATE	3. REPORT TYPE AND DATES COVERED
	November 1997	Phase III Technical Progress Report, 1 August 1996 - 31 July 1997

4. TITLE AND SUBTITLE

Amorphous Silicon Research, Phase III Technical Progress Report, 1 August 1996 - 31 July 1997

5. FUNDING NUMBERS

C: ZAN-4-13318-02
TA: PV704401

6. AUTHOR(S)

S. Guha

7. PERFORMING ORGANIZATION NAME(S) AND ADDRESS(ES)

United Solar Systems Corp.
1100 West Maple Road
Troy, MI 48084

8. PERFORMING ORGANIZATION REPORT NUMBER

9. SPONSORING/MONITORING AGENCY NAME(S) AND ADDRESS(ES)

National Renewable Energy Laboratory
1617 Cole Blvd.
Golden, CO 80401-3393

10. SPONSORING/MONITORING AGENCY REPORT NUMBER

SR-520-23543

11. SUPPLEMENTARY NOTES

NREL Technical Monitor: K. Zweibel

12a. DISTRIBUTION/AVAILABILITY STATEMENT

12b. DISTRIBUTION CODE

UC-1262

13. ABSTRACT ***(Maximum 200 words)***

This report describes the progress made by United Solar Systems Corp., during the third year of a research program to improve its understanding and capabilities for developing multijunction amorphous silicon alloy cells. Highlights of the work include investigating the effect of plasma chemistry and deuterated precursor gases on cell properties, optimizing component cells of the triple-junction structure, and developing stable triple-junction cells. Progress has been demonstrated in the performance of all the component cells, leading to the world-record achievement of stable 13% active-area efficiency using a triple-junction cell.

14. SUBJECT TERMS

photovoltaics ; amorphous silicon research ; multijunction a-Si alloy cells

15. NUMBER OF PAGES
4 43

16. PRICE CODE

17. SECURITY CLASSIFICATION OF REPORT	SECURITY CLASSIFICATION OF THIS PAGE	19. SECURITY CLASSIFICATION OF ABSTRACT	20. LIMITATION OF ABSTRACT
Unclassified	Unclassified	Unclassified	UL